Surface & Coatings Technology 307 (2016) 157–170

Contents lists available at ScienceDirect

Surface & Coatings Technology

journal homepage: www.elsevier.com/locate/surfcoat

Effect of ultrasonic nanocrystalline surface modification on the water droplet erosion performance of Ti—6Al—4V

Abdullahi K. Gujba [a], Zhencheng Ren [b], Yalin Dong [b], Chang Ye [b], Mamoun Medraj [a,c,*]

[a] Department of Mechanical and Industrial Engineering, Concordia University, 1455 De Maisonneuve Blvd. W. Montreal, Quebec, H3G 1M8, Canada
[b] Department of Mechanical Engineering, The University of Akron, Akron, OH 45325, USA
[c] Department of Mechanical and Materials Engineering, Masdar Institute, P.O. Box 54224, Masdar City, Abu Dhabi, United Arab Emirates

ARTICLE INFO

Article history:
Received 21 June 2016
Revised 17 August 2016
Accepted in revised form 18 August 2016
Available online 25 August 2016

Keywords:
UNSM
Microhardness
Compressive residual stress
WDE
Impact speed
Ti—6Al—4V

ABSTRACT

The effect of ultrasonic nanocrystalline surface modification (UNSM) on the water droplet erosion (WDE) performance of Ti—6Al—4V was studied. It was observed that UNSM induces deep levels of compressive residual stresses in both the scanning and transverse directions. The treated surface revealed microdimples in a micro-tracked fashion. Mechanical deformation marks were observed within the grains due to excessive plastic deformation and variation in grain size was observed across the ultrasonically modified layer. Microhardness of the UNSM condition was enhanced significantly as compared with the untreated (As-M) condition. The WDE performance tests for the UNSM and As-M conditions were conducted in a rotating disc rig in accordance with ASTM G73 standard. Influence of impact speed on WDE was explored on two different sample geometries (T-shaped flat and airfoil). WDE results showed that the flat UNSM samples had enhanced WDE performance at speeds 250, 275 and 300 m/s as compared with the As-M condition. At 350 m/s, both UNSM and As-M conditions showed similar performance. UNSM airfoil samples showed mild enhancement in the WDE performance at 300 m/s during the advanced stage as compared with the As-M condition. At 350 m/s, the UNSM airfoils do not show enhancement in WDE performance.

1. Introduction

In the power generation industry, the fogging method employed to cool the intake air into the compressor poses severe erosion damage to the leading edge of the blades. This occurs due to the synergy of the impacting water droplets and rotating blades. This is usually termed as "water erosion by impingement (liquid impingement erosion) or water droplet erosion (WDE)" [1]. WDE is the progressive loss of material from a solid surface due to accumulated impacts by liquid droplets [2]. WDE is a complex phenomenon due to many interacting parameters such as impact speed, droplet size, impact angle and conditions of the target material such as mechanical properties and surface roughness. The main causes of WDE damage are the high pressure exerted by the relative speed between the droplets and the rotating blade and the liquid lateral jetting [3]. The jetting is the radial outflow of the liquid droplets after impact which is identified as a major cause of the erosion damage [4]. Heymann [5] proposed four primary modes of WDE damage, which are plastic deformation and asperity formation, stress waves propagation, lateral jetting and hydraulic penetration. WDE consists of several stages *viz.*: incubation period where mass loss is negligible; acceleration stage (energy accumulation zone [6]) where mass loss is significant; maximum erosion rate stage where mass loss is at its peak and terminal or final steady state with erosion rate declining and remaining constant [5,7]. These stages are further affected by surface roughness [7], mechanical properties [4], microstructure [3], geometry [7] and combination of impact speed and droplet size [7]. In order to prolong the life span of components, the WDE performance of materials such as Ti—6Al—4V must be improved. Ryzhenkov et al. [8] stated that the methods of mitigating WDE can be classified into two distinct categories with certain conditions; (1) active (intrinsic) methods which basically minimize the main factors causing the erosion such as reducing the moisture content as well as decreasing the droplet sizes and; (2) passive (extrinsic) methods which aim at enhancing the surface and mechanical properties of blades' materials. The passive method has been adopted due to its economic feasibility [9]. Despite the efforts to combat or mitigate the erosion damage, it has not been possible to identify or quantify an absolute parameter for WDE resistance [10]. This is due to the fact that erosion rate is not constant with time and therefore, no single value can quantify the erosion performance.

Several surface modification techniques such as coatings [11,12] and laser surface treatments [13,14] have been employed to combat WDE. However, achieving this goal still remains a challenge due to the

* Corresponding author at: Department of Mechanical and Industrial Engineering, Concordia University, 1455 De Maisonneuve Blvd. W. Montreal, Quebec, H3G 1M8, Canada.
E-mail address: mmedraj@encs.concordia.ca (M. Medraj).

http://dx.doi.org/10.1016/j.surfcoat.2016.08.054
0257-8972/

presence of surface defects and microcracks after surface modification. Mechanical surface treatments such as deep rolling (DR) [15], has recently being explored in this regard. However, more work is still needed in order to fully understand the effectiveness of mechanical treatments in combating erosion damage. WDE damage is likened to fatigue-like damage due to fatigue striation marks caused by the cyclic nature of the liquid droplet impacts [4,15,16]. Researchers [17–19] have shown that WDE damage mechanisms is influenced significantly by crack initiation and propagation. It is well known that mechanical surface treatments retard crack initiation and propagation as well as enhance fatigue life [20]. Thus, one would expect mechanical surface treatments to combat WDE damage. However, the effect of cold working (strain hardening) before exposing the surface to liquid droplet impacts has been questioned. This is because the mechanical treatments plastically deform the surface and induce strain hardening. Repeated droplet impacts strain harden the material further [3]. Frederick and Heymann [3] stated that the duplication of the work hardening process might show detrimental effects and in another report by Heymann [4], he suggested the opposite trend with the condition that too much cold working should be avoided. To shed more light with regards these claims, a relatively new mechanical surface modification technique called ultrasonic nanocrystalline surface modification (UNSM) is explored. This technique harnesses ultrasonic vibration energy which converts harmonic oscillations of an excited body into resonant impulses of high frequency [21]. The generated energy from these oscillations are used to impact the work piece. Tungsten carbide (WC) [22,23] or silicon nitride ceramic (Si_3N_4) [21,24] ball tip that is attached to an ultrasonic horn is used to strike/impact the work piece surface at high frequency of up to 20 kHz [21]. Typical impacts on the work piece surface range from 20,000 to 40,000 shots per square millimeter [21]. Other process parameters include static load, number of impacts/strikes, intervals, amplitude and diameter of the ball tip. The high frequency striking of the ball leads to severe plastic deformation of the surface, thereby introducing high density of dislocations [23]. Hence, the top surface and in-depth of the work piece are modified, which improves the mechanical properties. The strengthening effect is due to the plastic strain and refined microstructure [25]. The microstructural refinement after UNSM treatment improves mechanical properties based on the Hall-Petch relationship [26]. Generally, UNSM treatment has shown increased hardness [23, 25,27,28], reduced grain size [29,30], improved surface quality [25] and deep levels of compressive residual stresses [21,25,28,31]. Based on the aforementioned attributes, UNSM has shown enhanced fatigue life [25,27,28,31], enhanced cyclic oxidation behaviour of coated Ni-based superalloy (CM247LC) [29], enhanced tribological properties such as wear resistance [21,24,30,32] and lowering of friction coefficients [21,24,30,32] of materials. To this point, no study could be found in the literature regarding the effectiveness of UNSM and the associated attributes on the WDE performance of Ti—6Al—4V or other alloys. Since UNSM process is known to enhance fatigue life of materials and WDE damage is ascribed to fatigue-like mechanism, studying WDE performance of UNSM treated Ti—6Al—4V is worthwhile.

In this work, the effect of UNSM on the WDE performance of Ti—6Al—4V was investigated for the first time. The microstructure, microhardness, induced compressive residual stresses were discussed in relation to the WDE performance. Much attention was given to the influence of impact speed on the WDE performance. The sample geometry is another factor that can influence WDE behaviour, however only flat sample geometry has been explored in the literature [11–15] and the effect of sample geometry on the WDE behaviour could not be found in the literature The current study addresses this issue by employing two different sample geometries (T-shaped flat and airfoil). Also, the influence of sample geometry and the effectiveness of UNSM treatment on the WDE performance of Ti—6Al—4V are addressed in this work. UNSM processing, sample characterizations and WDE tests are detailed in the following section.

2. Experimental procedure

2.1. Material and geometry

For the present study, Ti—6Al—4V (ASTM B265, Grade 5) alloy, a typical material for compressor blades in gas turbines, was investigated. Room temperature physical and mechanical properties of this alloy are: elastic modulus (113 GPa), Poisson's ratio (0.342), tensile strength (880 MPa) and melting temperature range (1604–1660 °C) [33]. T-shaped and airfoil samples, as shown in Fig. 1, were machined in accordance to the sample's geometrical requirement of the WDE testing rig. The T-shaped sample represents the typical flat surfaces commonly used in the literature [11–15]. However, in real gas turbine compressor blade where damage is caused by droplet impacts, the airfoil (aerofoil) geometry represents the leading edge of the compressor blade. For this reason, the airfoil geometry was used in this work. Fig. 2a and b show the starting microstructure of the Ti—6Al—4V alloy which contains α- and β-phases.

2.2. UNSM treatment and characterization

2.2.1. UNSM processing

The as-machined (As-M) samples (T-shaped and airfoil) surfaces were modified using UNSM apparatus at The University of Akron, Ohio, USA. The modified surfaces are indicated by the arrows in Fig. 1. The airfoil sample was treated on both sides in order to avoid sample distortion. This is the usual practice when applying mechanical surface treatments such as laser shock peening (LSP) on airfoil geometry [34]. UNSM process parameters are summarized in Table 1 and are also compared with other UNSM parameters found in the literature [21–23]. To observe the effectiveness of UNSM processing, several techniques were used to characterize the untreated and treated samples and are discussed in the following sections.

2.2.2. Surface roughness

Mitutoyo SJ-210 portable surface roughness tester was used to measure the surface roughness (*Ra*) before and after UNSM treatment. An average of 5–7 readings was taken across the sample surface. The surface roughness is an important parameter in WDE study because roughness can act as stress raiser or crack initiation sites [20]. Hence, it is recommended to have similar initial surface roughness when comparing the WDE performance of different materials and/or surface conditions.

2.2.3. X-ray diffraction pattern and residual stress measurement

X-ray diffraction (XRD) patterns for the untreated and UNSM treated surfaces were acquired in order to observe any phase changes/transformations due to UNSM processing. Phase change/transformation has been reported in material such as 304 stainless steel after UNSM processing [25,27,28,31]. In this work, the constituent α- and β-phases were monitored before and after processing. The compressive residual stresses before and after UNSM were also measured using the XRD $\sin^2\phi$ technique at Proto Manufacturing Inc., USA. Crystallographic plane of {213} and Bragg's angle ($2\theta = 142°$) obtained by Cu Kα

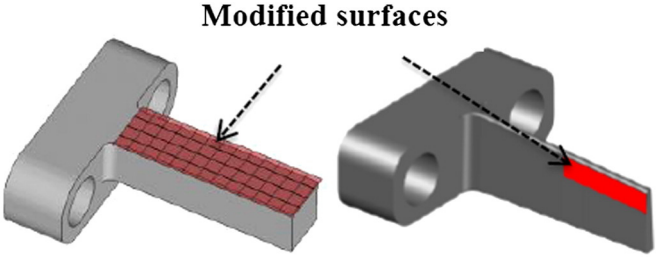

Fig. 1. Typical T-shaped flat (left) and airfoil (right) samples machined.

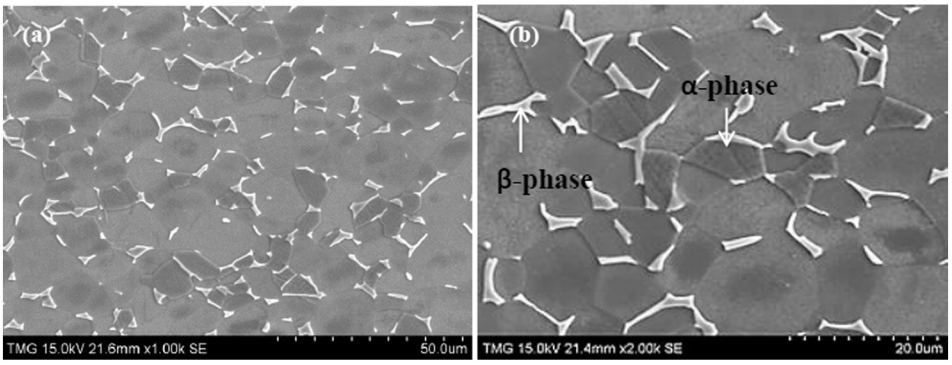

Fig. 2. SEM micrographs showing the initial Ti—6Al—4V microstructure at (a) lower and (b) higher magnifications.

radiation were used for this purpose. For the UNSM condition, the top surface and in-depth residual stresses were measured relative to the ultrasound scanning directions *i.e.* parallel (0°) and transverse (90°). For the sake of comparison, the top surface residual stresses for the As-M condition were also measured using these two directions. To quantify the residual stress values with respect to depth, surface layers were gradually removed by electropolishing. Strain gradient correction and layer removal corrections were carried out in accordance with SAE J784a standard [35]. Total depth of 0.26 mm was measured with initial fine steps of 0.03 mm down to 0.15 mm followed by two coarser steps of 0.06 mm down to 0.21 mm and of 0.05 mm down to 0.26 mm. More information on the residual stress measurements using the $\sin^2\phi$ technique can be found in the standard [35].

2.2.4. Microhardness

Microhardness measurements were carried out on the top surface and cross-section of all treated and untreated samples. A direct load of 50 gram-force (gf) and a dwell time of 15 s were used. Prior to the hardness measurements, the samples (treated and untreated) were cut perpendicular to the surface using a diamond cutter. Under cooling and lubricating fluid conditions, low speed and moderate load were applied in order to minimize unwanted surface modifications during cutting. After mounting, silicon carbide grit papers from 400 to 800 were used for grinding and vibratory polishing with 1 μm diamond paste was employed to remove scratches and other undesired debris.

2.2.5. Microstructure investigations

To observe any surface features such as microdimples, the as-treated top surface was observed under SEM (S-3400N, Hitachi). Also, the cross-section of the as-treated condition was observed using optical microscope. For surface and in-depth microstructure investigations, Kroll's reagent containing 2 ml HF + 5 ml HNO_3 + 100 ml H_2O was used to etch the vibratory polished samples. Etching time of 15 s was chosen in order to have a balance between details and contrast as recommended by Gammon et al. [36]. SEM images of the polished-etched top surface and cross-sections for both treated and untreated samples were taken at different magnifications.

2.3. WDE testing and characterization

2.3.1. WDE tests

A rotating disc rig available at Concordia University, shown in Fig. 3a, was used for studying the WDE performance of the treated and untreated Ti—6Al—4V. In this study, the untreated Ti—6Al—4V is used as a reference. Details about this unique erosion rig have been reported in [19, 37]. The test was conducted in accordance with the ASTM G73 standard [10]. In this rig, the untreated and UNSM treated samples were fixed at diametrically opposite ends of the rotating disc as shown in Fig. 3a. To avoid vibration during testing, difference in sample weight not exceeding 0.05 g was maintained. It is worth noting that the surface roughness of both treated and untreated samples was similar prior to testing. Two types of nozzles as shown in Fig. 3b were used depending on the geometry to be tested. A shower head nozzle was used for testing the airfoil samples, whereas a single streak nozzle was used for testing the T-shaped flat samples. Typical WDE testing parameters are summarized in Table 2. Once the desired rotational speed was obtained, the water droplets (de-ionized water) were introduced while controlling the flow rate. The setup enabled the droplets to impact the samples at 90° in a repetitive fashion. The impact angle of 90° causes the most severe water erosion damage [38]. The erosion exposure time depended on the impact speed, nozzle type and sample geometry. For instance, for the T-shaped flat, 1 minute constant time intervals were used in order to capture the early stages of the erosion process (initiation stage). Whereas, longer time intervals of 2, 3, 4, 6, 10, 12, 30, 60 and 75 mins were employed as the test progressed to the advanced stages of erosion. For the airfoil, intervals of 2, 3, 4, 6, 8, 10, 12, 15, 18, 20, 24 and 30 mins were used.

2.3.2. Water droplet erosion behaviour

During the WDE tests, experiments were halted at certain intervals and eroded samples were weighed using a balance having ±0.2 mg accuracy. Typical erosion curves such as cumulative mass loss *versus* exposure time/number of impingements, maximum erosion rate (ER_{max}) *versus* impact speed and number of impingement to erosion initiation *versus* impact speed were plotted. For satisfactory determination of the incubation period and ER_{max}, a three line representation method [5] demonstrated in Fig. 4a was used. In Fig. 4a, the ER_{max} denoted as

Table 1
UNSM processing parameters for Ti—6Al—4V and study purpose.

Reference	Ball material	Diameter of ball tip (mm)	Frequency (kHz)	Interval (mm)	Amplitude (μm)	Study purpose
Amanov et al. [21]	Silicon nitride	2.38	20	0.07	30	Fretting wear and friction reduction
Cho et al. [22]	Tungsten carbide	2.30	20	0.07	30	Fatigue behaviour
Ye et al. [23]	Tungsten carbide	2.60	20	[a]	[a]	Mechanical properties and microstructure
Present work	Tungsten carbide	2.40	20	0.01	24	Water droplet erosion performance

[a] Indicates no information from the reference.

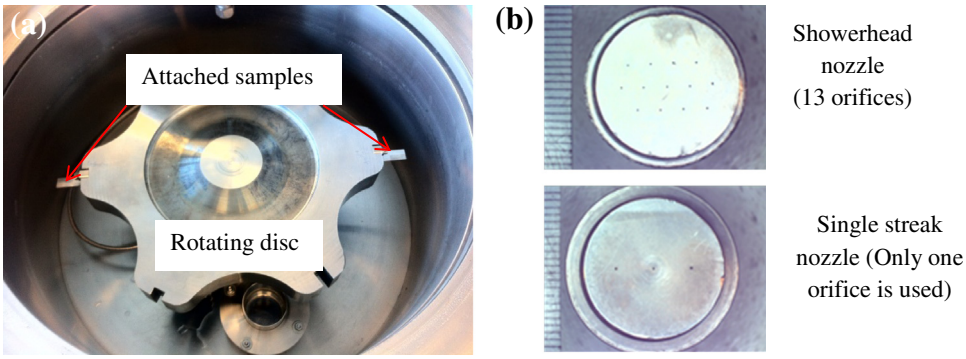

Fig. 3. Water erosion rig (a) and nozzles used (b).

"B" is the slope of the best line fit of the data points in the maximum erosion stage, whereas the incubation period denoted as "A" is the intersection of the straight line with the x-axis (exposure time axis) [10]. To observe the erosion rate as the erosion test progressed, the instantaneous erosion rate (ER_{inst}) which is the slope between two consecutive points on the erosion-time graphs were plotted (Fig. 4b). It is important to note that the incubation period, ER_{max} and ER_{inst} are analyzed in this study. To understand how the erosion process evolved, images were taken using a standard stereo optical microscope at the intervals during which mass loss was measured.

3. Results and discussion

3.1. Effect of UNSM on surface and in-depth characteristics

UNSM treatment has been considered as an effective and economically viable method for producing nano-corrugated [39] and nanostructured [32] surface layers. This is due to the accompanied grain refinement. Properties and microstructure of the modified layers can be controlled by careful selection of process parameters such as static load, amplitude, diameter of the ball tip and interval. In this study, interval of 0.01 mm, static load of 30 N, amplitude of 24 μm and tip diameter of 2.4 mm were used for the UNSM treatment. The effect of UNSM process on the surface roughness, XRD pattern, compressive residual stress, microstructure and microhardness were investigated and reported in this paper.

3.1.1. Surface roughness

The average surface roughness (*Ra*) values before and after UNSM treatments were recorded. Five different locations across the treated and untreated surfaces were measured and average *Ra* value was taken. *Ra* values of 0.71 ± 0.06 μm and 0.26 ± 0.02 μm were observed before and after UNSM, respectively. It can be seen that the surface roughness after UNSM treatment was reduced significantly (about 63% reduction). Also, the UNSM showed a relatively uniform roughness across the surface. This observation is also in accord with the findings of [24–26,30,32,40]. The surface roughness can further be controlled by varying parameters such as static load [21] and number of strikes [26]. It can be said that UNSM treatment improves surface quality. However, this is not the case in other processes such as shot peening (SP) and LSP where the control of surface roughness and surface defects is still a challenge [20]. For comparative studies such as wear and fatigue behaviour of materials, the surface roughness of treated and untreated samples should be made comparable [24,25,27]. To study WDE, the untreated samples were also polished to a comparable surface roughness similar to the UNSM samples. An average *Ra* value of 0.25 ± 0.03 μm is used for the untreated samples in this work and more on this is discussed in Section 3.2.

Table 2
WDE test parameters used in the present work.

WDE parameters	Flat sample	Airfoil sample
Impact speed (m/s)	250, 275, 300, 350	300, 350
Rotational speed × 10^3 (rpm)	10, 11, 12, 14	12, 14
Flow rate (l/min)	0.05	0.15
Nozzle head type	Single streak	Shower head
Stand-off distance (mm)	5	5
Average droplet size (μm)	463	460
Impact angle (°)	90	90

3.1.2. XRD pattern and compressive residual stresses

The XRD patterns of the untreated and UNSM conditions are as shown in Fig. 5, where reduced peak intensity and peak broadening are observed for the UNSM condition compared with the untreated material. Full width half maximum (FWHM) approach was employed to quantify the peak broadening. For instance, analysing the first three peaks in Fig. 5, FWHM values were quantified. For the untreated condition, 0.26, 0.22 and 0.36 were obtained for first, second and third peaks, respectively. Similarly, for the treated condition, 0.48, 0.48 and 0.55 were obtained. It has been reported that reduced peak intensity and peak broadening are due to the high induced strains, causing severe plastic deformation and grain refinement [41–43]. Fig. 5 clearly indicates that UNSM treatment is one of such processes that induce severe surface layer of plastic deformation.

The compressive residual stresses in the 0 and 90° directions before and after UNSM were measured. Surface of the As-M condition showed −490 ± 19 MPa and −607 ± 9 in the 0 and 90° directions, respectively. The UNSM surface showed −863 ± 18 MPa and −1582 ± 28 in the 0 and 90° directions, respectively. UNSM condition showed higher top surface compressive residual stress in both directions than the As-M condition. This is due to the local plastic deformation and induced strain hardening during UNSM processing [31]. Similar top surface residual stress has been observed elsewhere on UNSM-treated Ti—6Al—4V [21]. Also, due to machining, grinding and polishing, the observed surface compressive residual stresses for the untreated condition is expected. Chou et al. [44] demonstrated that surface finishing techniques such as grinding and polishing can induce different levels of compressive residual stresses. Variation of the compressive residual stress with depth was measured for the UNSM condition. Fig. 6 shows the observed stress profile and it can be seen that compressive residual stresses were induced into the material down to 0.25 mm. Similar variation in residual stress has been reported on UNSM treated Ti—6Al—4V [21,22]. Depth of compressive residual stress down to 0.15 mm [21] and 0.16 mm [22] was observed. It is also shown that the stresses in 0 and 90° directions were different. For instance, comparing the magnitude of the compressive residual stresses from the top surface to 0.12 mm depth, stresses in 90° direction were higher than in the 0° direction. However, beyond 0.12 mm depth, residual stresses in both directions were relatively similar. The observed compressive residual stresses induced *via* UNSM are due to the surface and sub-surface deformation. Compressive

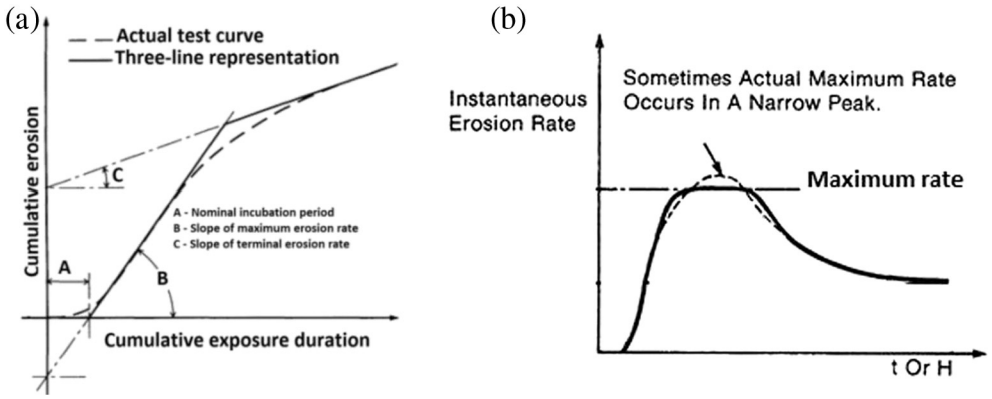

Fig. 4. WDE curve characterization using (a) three line representation [5] and (b) ER_{inst} [10].

residual stresses extend into the subsurface of the target material through dislocations multiplications and their interactions [20]. It has been pointed out that increasing the frequency of ball striking and load increases the macroscopic compressive residual stresses [23,26]. Contrarily, a decrease in compressive residual stresses was observed after applying very high static load [27]. Hence, careful selection of process parameters is required for optimized UNSM process.

3.1.3. Microstructure characteristics

The SEM micrographs in Fig. 7 show that UNSM treatment produces microdimples and microtracks on the surface. Microdimples are indentations produced due to the ball impact which causes severe plastic deformation during processing [32,40]. They are usually 1–2 μm in diameter [45] and formed in a micro-tracked fashion (Fig. 7) which can be attributed to the controlled processing parameters such as scanning interval. However, varying the interval induces different microtracks and microdimples patterns and consequently, different material properties/behaviours [46]. Microdimples have shown significant effect on tribological characteristics such as reducing the friction coefficient and the wear volume loss [45].

Also, due to the severe plastic deformation during UNSM processing, surface and sub-surface layers in the material are significantly changed. Fig. 8a shows optical macrograph of the cross section after UNSM treatment, whereas Fig. 8b shows a schematic illustration of the layers of a typically UNSM modified material.

The modified region in Fig. 8a indicates that the coarse-grain structure has been deformed significantly [45]. It can be seen from Fig. 8a that the effectiveness of the UNSM treatment is reduced with respect to the depth. In other words, an increase in the grain size away from the deformed region until the unaffected region is observed as shown in Fig. 8b. The grain refinement, in conjunction with the accumulation of dislocation, causes the enhancement in mechanical properties such as microhardness. Similar to other mechanical surface treatment techniques such as LSP, SP, DR and LPB, plastic deformation and induced strain after UNSM occur in a gradient manner, with the top surface showing the highest plastic strain followed by a gradual decrease into the material [31]. It is important to note that the plastically deformed layer shown in Fig. 8a could be increased by increasing the striking number and/or amplitude [23]. However, over processing may deteriorate the desired properties too.

Fig. 9a, b shows the polished and etched top surface of the untreated and treated samples. Fig. 9a shows un-deformed grains and the β-phase is surrounding the α-phase in a uniformly distributed fashion. However, Fig. 9b shows fragmented and elongated β-phase and the grain boundaries were less apparent. This could be due to the deformation of grains that resulted in the modified microstructure. Amanov et al. [21] also reported similar modified microstructure in Ti—6Al—4V after UNSM with the grain boundaries less apparent. Their [21] micrographs showed that the initially continuous β-phase was fragmented. Mechanical deformation marks in the grains were formed (Fig. 9b–d) after UNSM treatment due to the induced high strain and strain rate [23]. Location A in Fig. 9c and d clearly show the formation of the deformation marks within the grains. Fig. 9e and f show the cross-sectional micrographs of the untreated and treated conditions, respectively. Fig. 9e shows relatively un-deformed grains across the depth, whereas Fig. 9f shows the deformed or modified layer of about 30–40 μm at the top surface. This is attributed to the effectiveness of the UNSM technique in producing relatively deep modified layers.

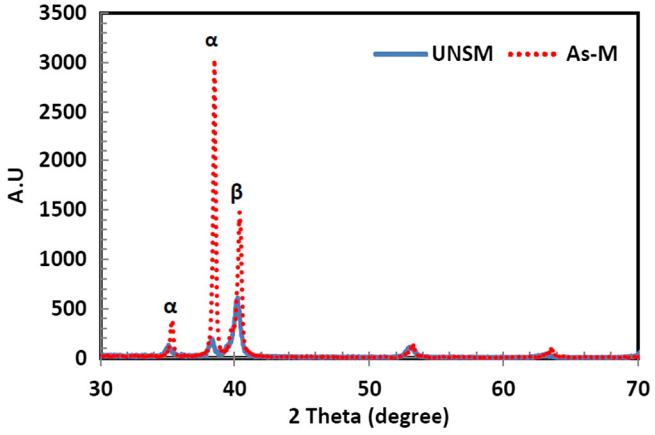

Fig. 5. XRD patterns for the As-M and UNSM treated surface.

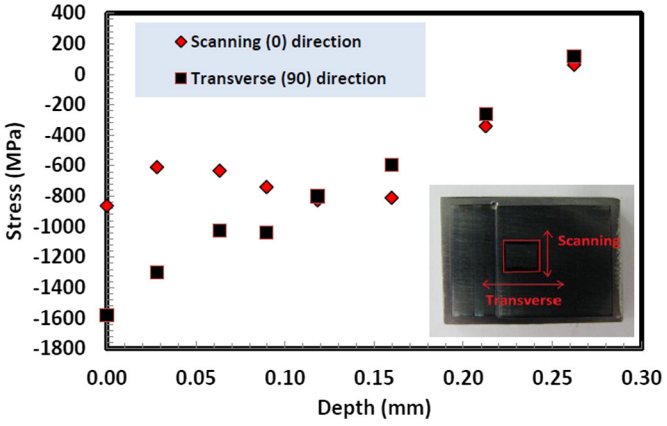

Fig. 6. Variation of top surface and in-depth compressive residual stress profile.

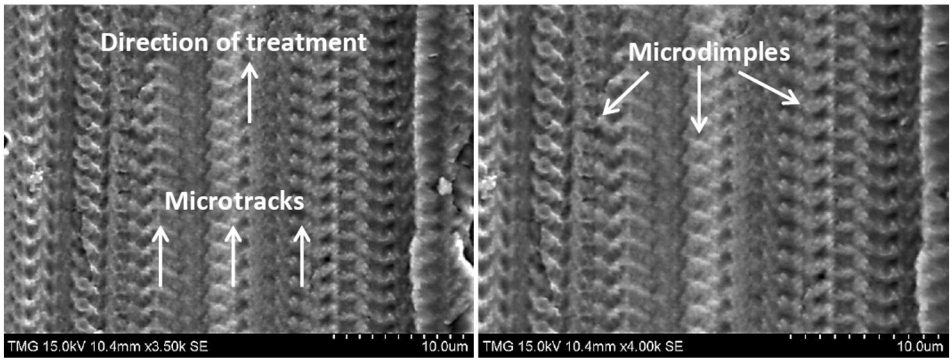

Fig. 7. SEM micrographs showing microtracks and microdimples on ultrasonic modified surface.

3.1.4. Microhardness

As mentioned in Section 2.2, a 50 gf load was used to measure the top surface and in-depth microhardness. Microhardness at 7–8 locations were obtained across the depth of UNSM and As-M samples. At each location, the average and standard deviation of 4–5 readings were calculated. Fig. 10 shows the microhardness values for untreated and UNSM conditions. It is clear that the UNSM condition showed enhanced microhardness as compared with the untreated condition. The top surface microhardness values were 331 ± 5.3 HV and 379 ± 7.6 HV for untreated and UNSM conditions, respectively. Furthermore, the microhardness can further be enhanced by varying UNSM parameters such as scanning interval [21] and number of strikes [26]. This increases the depth of the deformed layer, thus increasing the microhardness [23,26]. It is important to note that the highest microhardness value of 427 ± 16.83 HV was observed 30 μm below the top surface. This is also shown in the optical macrograph embedded in Fig. 10. To confirm the aforementioned trend, another treated sample was measured and similar microhardness trend was observed. Amanov et al. [21] also reported similar variation in microhardness below the surface of UNSM treated Ti—6Al—4V. This could be due to the additional work hardening during cutting, polishing and grinding. Zaden et al. [47] showed microhardness increase below the surface of Al6061 after cutting in dry, wet and mist conditions. They [47] attributed this trend to the increase in surface deformation which further increased the work hardening effect. For the treated conditions, the microhardness values decreased steadily after the plastically deformed layer. In general, the increase in microhardness after UNSM can be attributed to the grain refinement and work hardening effect. This observation is in accord with UNSM treatment on Ti—6Al—4V [22,23], medium carbon steel (S45C) [26], austenitic stainless steel (SUS 304) [27] and magnesium alloy (AZ91D) [30]. Hence, the surface and in-depth features observed in Figs. 5–10 are used to help understand the WDE performance of the As-M and UNSM conditions. The WDE results are detailed in the following section.

3.2. Water droplet erosion

Prior to the WDE tests, the As-M flat samples were polished to a similar surface finish as the UNSM samples. The average *Ra* for the polished and UNSM samples were approximately 0.25 ± 0.03 μm and 0.26 ± 0.02 μm, respectively. This was done because the presence of surface defects or imperfections such as scratches has an influence on the WDE behaviour of materials. Heymann [7] emphasized the influence of surface roughness on the erosion behaviour of materials. He [7] stated that the presence of surface asperities or irregularities facilitates the erosion initiation. This is because irregularities on the surface act as stress raisers and potential sites for pit formation and growth. Also, due to the high speed lateral jetting which interacts with surface irregularities or asperities, further crack initiation and material damage are observed. Hence, better surface quality delays the crack initiation and material damage. For instance, Kirols et al. [48] studied the influence of initial surface roughness on the WDE behaviour of 12%Cr-steel and Ti—6Al—4V. For the Ti—6Al—4V, samples with average initial surface roughness values (*Ra*) of 0.30, 0.12 and 0.04 μm were tested. They [48] reported that merely polishing the surfaces prior to WDE tests delayed the erosion initiation and decreased the maximum erosion rate. In this work, polishing was done in order to reduce the effect of surface roughness.

For the T-shaped flat samples, UNSM *versus* the polished As-M samples were tested. For simplicity, the polished-As-M samples are referred to As-M (untreated) samples for all the WDE tests. At each WDE testing condition (mentioned in Table 2 and Section 2.3.1); two coupons (As-M and UNSM) were tested at the same time in order to investigate their WDE performance. The main parameter that was varied was the impact speed while keeping other parameters constant. Here, impact speeds of 250, 275, 300 and 350 m/s were selected. This is because the predominant factor in the material damage is the impact speed [19,49]. This is attributed to the increased kinetic energy ($\frac{1}{2}mv^2$) with increasing the

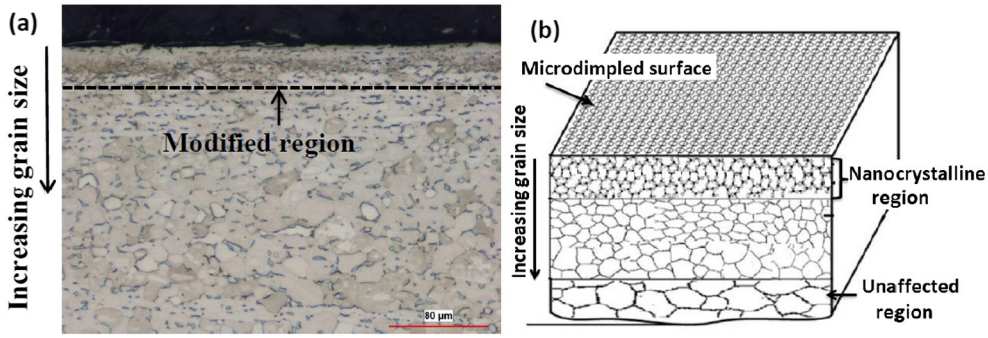

Fig. 8. (a) Optical macrograph of typical UNSM sample and (b) schematic illustration of structure characteristics and grain size profile on UNSM treated condition.

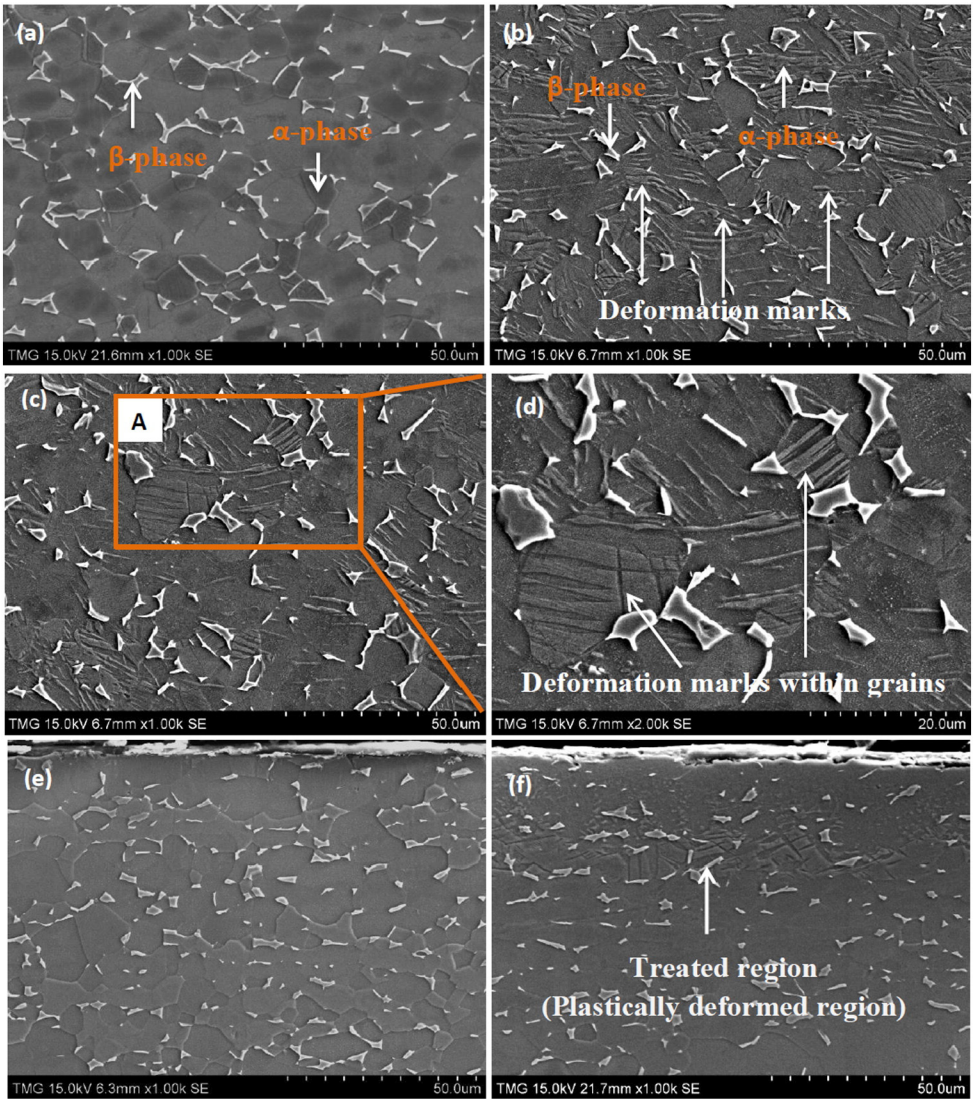

Fig. 9. SEM micrographs showing polished and etched (a) untreated top surface, (b, c, d) UNSM treated top surface, (e) untreated cross-section and (f) UNSM treated cross-section.

speed. The cumulative mass losses *versus* the number of impingements graphs were plotted. The number of impingement was determined using Eq. (1).

$$N_{imp} = R \times E_t \times N_{droplets} \quad (1)$$

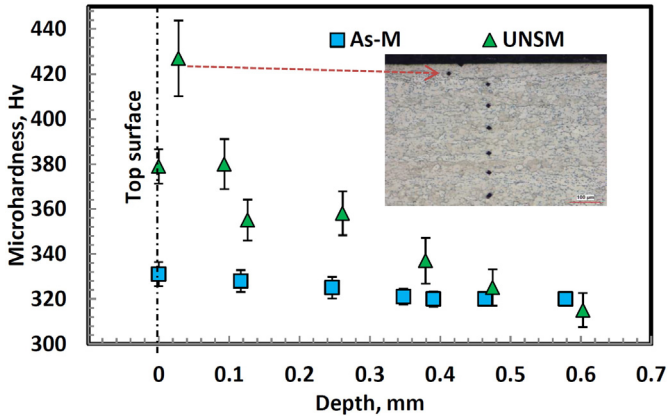

Fig. 10. Variation of microhardness with depth for treated and untreated samples.

where N_{imp} is the cumulative number of impingements during an exposure period, R is the rotational speed (rpm), E_t is the erosion exposure time (mins) and $N_{droplets}$ is the number of droplets impacting the sample per revolution. For the flat sample geometry in this work, $N_{droplets}$ is 6. Detailed procedure on the droplet generation, droplet size distribution and number of droplets hitting the sample can be found in reference [19]. For the airfoil samples, only impact speeds of 300 and 350 m/s were used. Here, 350 m/s was chosen as the most severe condition, whereas 300 m/s was chosen in order to have a less severe testing condition and also, to avoid prolonged testing. Tests using impact speed of 250 and 275 m/s for airfoil geometry would mean testing for prolonged erosion time without significant mass loss. Therefore, tests at these speeds were not performed. Contrary to the flat sample geometry, there is a challenge of quantifying the number of droplets hitting the airfoil sample. This is due to the shower head nozzle used during testing. Hence, graphs of cumulative mass loss *versus* number of cycles were plotted. The number of cycles is simply the rotational speed (rpm) multiplied by the erosion exposure time (mins). It is worth noting that the amount of water used after certain time interval can be computed by multiplying the number of cycles by the flow rate.

It is worth mentioning that there are two threshold speeds in relation to erosion damage *i.e.* first and second threshold speeds [19]. The first threshold speed is the speed below which no apparent damage is seen. However, the definition of this speed is somehow subjective and

depends on the testing conditions such as impact speed, droplet size and number of impingements. More information regarding first threshold speeds with regard to different applications such as liquid impingement erosion for pipe wall thinning, liquid jet impact, WDE for compressor blade applications has been addressed by the authors in [19]. The second threshold speed is the speed at which mass loss is measurable. In this work, all the selected impact speeds are speeds at which measurable mass losses are observed.

In order to verify the repeatability of the WDE experiments, tests at 250 and 350 m/s with 463 μm droplet size were conducted. For each test speed, the samples had similar surface quality and each test was conducted twice. Also, for each test speed, the two tests are designated as test 1 and test 2. Fig. 11 shows the WDE curves for test 1 and test 2 for both speeds. It can be seen that for each test speed, the curves coincided for most of the data points, indicating an acceptable level of repeatability.

3.2.1. WDE performance of UNSM and As-M T-shaped sample conditions

Fig. 12 shows the cumulative mass loss *versus* number of impingements graphs for the flat samples. The graphs compare the WDE performances of UNSM and As-M samples tested at different speeds. Fig. 12a shows that similar WDE performance was observed at 350 m/s for UNSM and As-M samples. In other words, both conditions are exhibiting similar erosion trend in terms of initial mass loss and subsequent stages. This can be attributed to the severity of the WDE test conditions. Therefore, the UNSM treatment showed little or no beneficial effect in enhancing WDE performance at such high impact speed. At 300 m/s (Fig. 12b), UNSM showed a much better WDE performance as compared with the As-M condition. At 275 and 250 m/s (Fig. 12c, d), UNSM condition showed significant improvement in WDE performance at all stages of the erosion process as compared with the As-M condition. Based on the graphs shown in Fig. 12, the effect of UNSM treatment on the WDE performance of Ti—6Al—4V was observed at impact speeds of 250, 275 and 300 m/s. However, this was not the case at impact speed of 350 m/s.

Based on the three line representation (Fig. 4a), the influence of impact speed on the erosion initiation and ER_{max} is shown in Fig. 13a and b, respectively. It can be seen from Fig. 13 that reducing the impact speed from 350 to 250 m/s delayed the erosion initiation time and showed less ER_{max}. In other words, as the speed is decreased from 350 to 250 m/s, more droplet impingements are required in order to initiate erosion damage in both conditions. Comparing the As-M and UNSM conditions at 250 m/s, 6 million droplet impingements were required for erosion initiation for the UNSM condition as compared with 2.1 million droplet impingements required for the As-M condition, indicating better WDE performance of the UNSM condition at this speed. As the impact speed is increased, the number of impingements for erosion initiation is significantly reduced for both conditions. At 350 m/s, the number of impingements to initiate erosion for the UNSM and As-M samples was the same, indicating the effect of the speed on the erosion initiation. When comparing the ER_{max} for the UNSM and As-M samples (Fig. 13b), UNSM condition showed less ER_{max} at impact speeds ≤300 m/s as compared with the As-M condition. However, at 350 m/s, both conditions showed similar ER_{max} due to the severity of the erosion test. The relationship between erosion rate and impact speed has been discussed and emphasized in the literature [6]. This dependency between the maximum erosion rate and impact velocity can be expressed using Eq. (2). Based on the power law relationship in Eq. (2), the speed exponent n can be determined.

$$ER_{max} \propto V^n \tag{2}$$

where ER_{max} is the erosion rate, V is the impact speed and n is the speed exponent. For metals, typical exponent values range from 5 to 7 in the literature [6,49]. However, based on Fig. 13b, exponent values of 11.2 and 12.1 were observed for the As-M and UNSM samples, respectively. The values observed in this study are different from the values observed by Kamkar [17] and Mahdipoor et al. [37] for Ti—6Al—4V. This discrepancy can be attributed to the test conditions, initial surface quality of the samples and the starting microstructure. The higher value shown by the UNSM condition indicates higher dependence on impact speed and more sensitive to the change in speed than the As-M condition. The impact damping capacity and fracture toughness of the UNSM surface are reduced. This hypothesis is in accord with the explanation given by Ma et al. [15] in their study on the WDE performance of deep rolled Ti—6Al—4V.

Interestingly, using the instantaneous erosion rate approach (Fig. 4b), the variation of erosion rates with increase in exposure could be traced clearly. Fig. 14a–d shows the ER_{inst} *versus* number of impingements at different speeds. It can be seen that the As-M condition had higher ER_{inst} and maximum ER_{inst} than the UNSM condition at all speeds. The maximum ER_{inst} is the highest points on the graphs (Fig. 14). At 350 m/s, the ER_{inst} were very close for both conditions. Also, Fig. 14 shows that the maximum ER_{inst} was not reached after the same number of impingements/exposure for the UNSM and As-M conditions. In other words, the As-M condition reached its maximum ER_{inst} much earlier than the UNSM condition. Table 3 shows the aforementioned maximum ER_{inst} trends and the number of impingements at which the maximum ER_{inst} occurred for the treated and untreated conditions. Table 3 indicates that UNSM condition required more droplet impingements to reach its maximum ER_{inst} at all speeds. It is important to note that this insight is missed by the three line representation (Fig. 4a) because it only uses a straight line to determine the ER_{max}. Therefore, for comparative erosion studies, it is recommended to observe and report the ER_{inst}.

Based on Figs. 12 and 14 and Table 3, the general trend is that UNSM (T-shaped) samples showed enhanced WDE performance than the As-M samples at impact speeds 250, 275 and 300 m/s. However, at 350 m/s, both treated and untreated conditions showed similar WDE performance. This trend is in accord with the observations of Mahdipoor et al. [11] where they studied the WDE performance of HVOF sprayed coated and uncoated Ti—6Al—4V. Impact speeds of 250, 300 and 350 m/s were employed and their [11] results showed that at speed of 250 m/s, the coated condition had enhanced erosion performance compared to the uncoated condition. At 350 m/s, similar erosion performance was observed for the coated and uncoated conditions [11]. In another study, Mahdipoor et al. [37] studied the influence of impact speed on water droplet erosion of TiAl (Titanium Aluminide) compared with Ti—6Al—4V. They [37] showed that TiAl had superior WDE performance compared to Ti—6Al—4V at 275 and 300 m/s impact speeds. Again, at 350 m/s, they [37] showed that the superiority of TiAl over Ti—6Al—4V was reduced significantly.

In this study, as the impact speed is increased from 300 to 350 m/s, the effectiveness of the UNSM treatment diminished. This can be attributed to the increased impact pressure which induced high internal

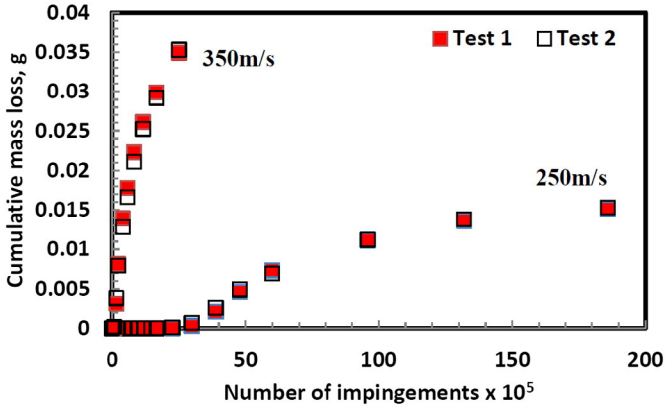

Fig. 11. WDE curves showing the repeatability of the results at 250 m/s and 350 m/s.

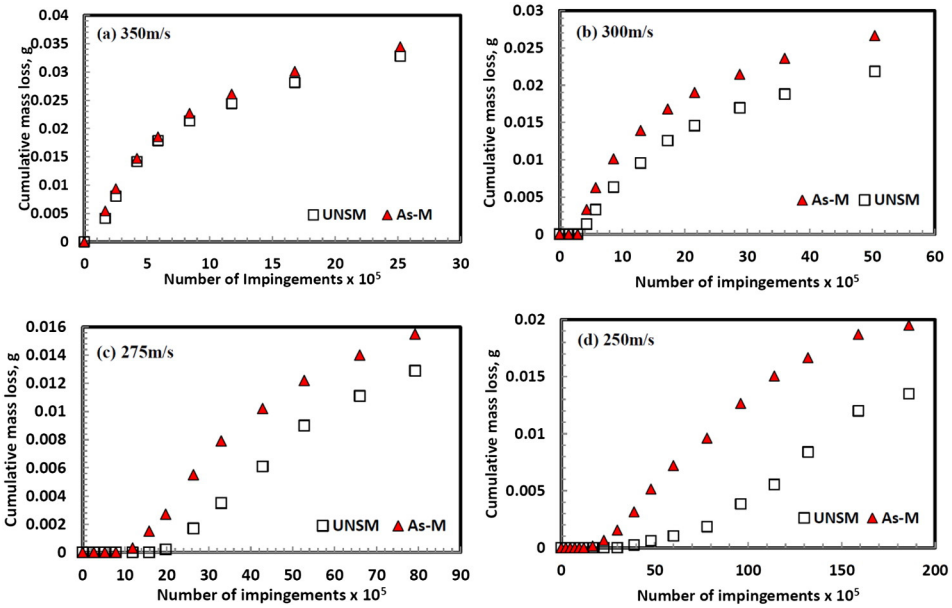

Fig. 12. WDE curves of As-M *versus* UNSM flat samples at different impact speeds.

stresses. This pressure is usually termed as 'water hammer pressure' which is the induced pressure exerted by the "arrested" liquid droplet on the solid surface. This observation is in accord with the explanation given by Thiruvengadam and Rudy [6], Mahdipoor et al. [11,37], Ma et al. [15] and Kamkar [17]. The exerted pressure strongly depends on the impact speed employed. Sanada et al. [50] reported that pressure distributions depend on Mach number (*Mi*) ranges. They [50] stated that the difference in pressure at the center and edge of the droplet is minimum for low *Mi* (between 0.1 and 0.4). For high *Mi* (>0.4), the edge pressure is 3 times that of the center when liquid jetting occurs [51,52]. In this study, the calculated Mach number is within the low *Mi* range. Moreover, high *Mi* range will only be achieved at impact speeds >550 m/s based on the assumptions in [50]. Nevertheless, the initiation period will be influenced greatly by the exerted impact pressure. According to Heymann [5,53], this pressure can be considerably higher than the yield strength of many alloys especially at high impact speeds. For instance, Eq. (3) provides a reasonable critical impact pressure by incorporating the shock wave velocity for rigid and elastic surface [53].

$$P = \rho C V\left(2 + \frac{(2K-1)V}{C}\right) \tag{3}$$

where P is the pressure (MPa), ρ is the density of the liquid (kg/m^3), C is the acoustic velocity of the liquid (m/s), V is the impact velocity (m/s), and $K = 2$ for water up to impact Mach number of 1.2. Incorporating values of 250 m/s, 275 m/s, 300 m/s and 350 m/s for V; water hammer pressures of 919, 1032, 1148 and 1392 MPa were obtained, respectively. Based on the calculated pressure values, it can be seen that the impact pressure increases linearly with the impact speed. Due to the high pressure at high speeds, the effectiveness of the UNSM treatment will be reduced significantly. For this reason also, similar erosion initiations for both the UNSM and As-M samples were observed for impact speeds 350 m/s (Fig. 12).

Highlighting the phenomenon of stress wave propagation could possibly explain the observed trends in Fig. 12. During the initial droplet impacts, part of the impact energy transmits through the solid until it reaches a discontinuity. This discontinuity can either be grain boundaries, inclusions and/or cracks. In this work, the deformed region due to UNSM treatment represents a discontinuity. At the discontinuity interface, part of the stress wave travels as transmitted waves, whereas the remaining part travels back in the opposite direction as reflected waves. As the erosion process evolves, the surface is continuously impacted by the liquid droplets and the transmission and reflection of the stress waves occur repeatedly. Hence, the transmitted and reflected waves interaction results in high tensile stress waves that cause crack initiation and propagation of existing cracks [15]. Due to the high frequency of the liquid impacts at high speeds, the stress wave interactions will be very fast and the magnitude of the resulting tensile stress waves will be high. However, the stress wave interactions will be reduced

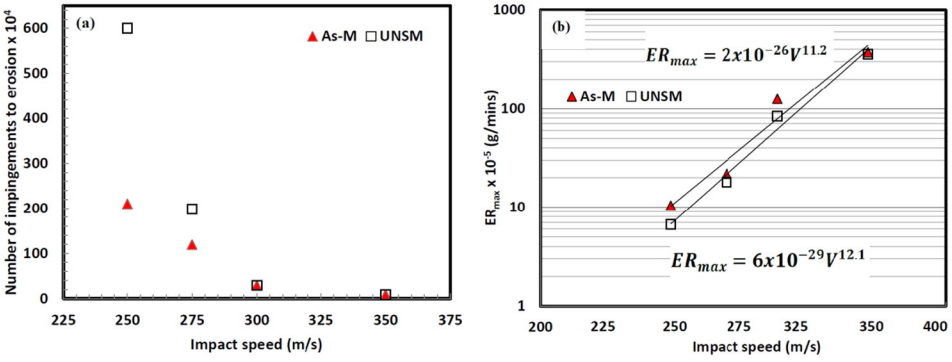

Fig. 13. Effect of impact speed on (a) number of impingements to initiation and (b) ER_{max}.

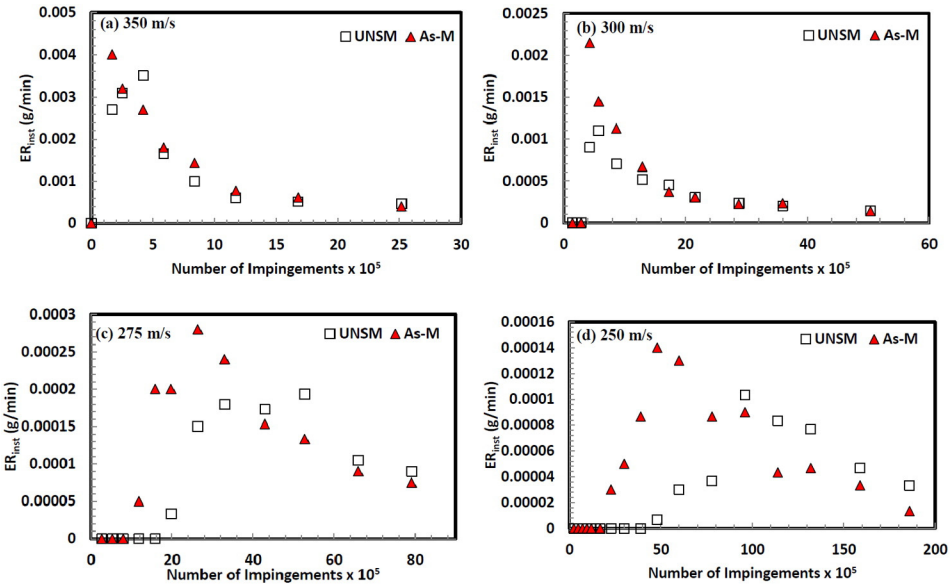

Fig. 14. ER_{inst} *versus* number of impingements at different impact speeds.

greatly as the impact speed is reduced, thereby reducing the magnitude of tensile stress wave. This is the scenario when the impact speed was reduced from 350 m/s to 250 m/s, where the effectiveness of the treatment was realized.

The enhanced WDE performance observed in this study at speed 250, 275 and 300 m/s are mainly attributed to the increased microhardness and modified microstructure. Heymann [4,7] stated that microhardness is a good and reliable material property used in assessing the resistance of materials to erosion damage. Reports [4,38] have shown that the erosion resistance varies with 2nd to 3rd power of Vickers hardness number. More so, refined microstructure or reduction in grain size has also been associated with erosion resistance of materials [38,54]. Materials having small finely distributed and hard particles are resistant to erosion especially in elastic and ductile matrix [4]. For treated Ti—6Al—4V, microhardness and refined microstructure have been considered among the most influential parameters improving the WDE performance. For instance, Yasugahira et al. [55] studied the water erosion resistance of pure Al and a range of titanium alloys. They [55] attributed the higher resistance of Ti alloys to the high Vickers number. Similar investigation was carried out by Robinson et al. [56] who reported that the resistance was due to the 10% increase in hardness and the refined microstructure. In this work, it has been shown that UNSM treatment enhanced the surface and in-depth microhardness (Fig. 10) and the modified surface and in-depth microstructure (Figs. 8a, 9b–d). For these reasons, UNSM condition showed enhanced WDE performance as compared with the As-M condition at speeds <350 m/s. The effect of micro-dimpled surface (Fig. 7) might also have contributed to the enhanced WDE performance. This is due to the fact that micro-dimpled surface has shown enhanced tribological characteristics. For instance, Amanov et al. [45] studied the influence of micro-dimples on the tribological behaviour of thrust ball bearing in a ball-on-disc test rig. The upper ring of the thrust bearing was used as the disc specimen and a rotational speed of 100 rpm was employed. Comparing the UNSM treated surface with ground surface, their [45] results showed that UNSM treated (micro-dimpled) surface had reduced wear volume loss as compared to the ground surface. Also, the friction coefficient of the UNSM-treated surface was reduced by about 25%. The effect of micro-dimples might be extended to WDE applications especially at very low speed such as 150 m/s. However, more experimental work is needed.

Since UNSM treatment involves work hardening similar to SP, LSP, LPB and DR, it enhances mechanical properties such as hardness. Heymann [4] stated that processes involving work hardening such as pressing, rolling or hammering might be beneficial in resisting erosion damage. However, excessive work hardening might show detrimental effects. In another report, Frederick and Heymann [3] stated that processes involving peening might not be very effective in enhancing the WDE behaviour of materials especially during the incubation stage. They [3] argued that the peening process involves plastic deformation which work hardens the surface and during droplet impingements, repeated plastic deformation further work hardens the surface. The duplication of the work hardening process at the incubation period might be detrimental to the WDE behaviour [3]. Heymann [7] further stated that the first plastic deformation retards erosion initiation while the second promotes the erosion initiation. The first and second plastic deformations balance each other, thus a non-enhanced WDE performance will be observed. Ma et al. [15] reported the WDE performance of untreated and deep rolled Ti—6Al—4V. Despite having improved hardness after the deep rolling process, both the untreated and treated conditions had the same WDE performance. They [15] suggested that there are two competing mechanisms at the initiation stage which balance out one another. These competing mechanisms are the work hardening process from the deep rolling process and the compressive residual stresses. While work hardening decreases the erosion resistance due to the increased brittleness, the presence of compressive residual stresses is expected to improve WDE resistance by delaying crack propagation. For this reason, no enhanced WDE performance was observed for the deep rolled treated condition. This is in accord with explanation given in [7] who pointed out that a non-enhanced WDE performance maybe observed due to duplication of the working hardening process. However, the results presented in this work showed contradictory trends to the arguments in [3,7]. For instance, changing the severity of erosion test conditions such as varying impact speed, different erosion

Table 3
Characterization of the ER_{inst} curves at various speeds.

Impact speed (m/s)	Condition	$ER_{inst} \times 10^{-5}$	$N_{imp} \times 10^5$
250	As-M	14	48
	UNSM	10	96
275	As-M	28	26
	UNSM	19	53
300	As-M	215	4
	UNSM	110	6
350	As-M	400	2
	UNSM	350	4

behaviour may prevail. This is the situation observed in this work where enhanced WDE performances were seen at speeds <350 m/s. Contrary to Frederick and Heymann [3], the incubation (erosion initiation) stage (Fig. 13a) in this work was significantly delayed for the UNSM treated sample at such varied conditions. Moreover, the ER_{max} (Figs. 13b and 14) was reduced significantly at these conditions. It can be inferred that the severity of the erosion conditions must be taken into consideration when evaluating the suitability of certain service treatment to combat WDE.

Another reason for the observed trends in this study and [15] is the level of induced plastic deformation during UNSM and DR processing. It might be that the amount of plastic deformation from the DR technique is higher than the UNSM technique. Due to the increased strain hardening, the DR treated material will be more brittle than the UNSM treated material. In this case, the UNSM condition will accommodate more plastic deformation from water hammering than the DR condition during the initiation stage.

It has been shown that UNSM induced deep levels of compressive residual stresses (Fig. 6). However, it is not guaranteed that the induced stresses are beneficial in enhancing WDE resistance. In this case, extensive work is still needed in order to fully understand the influence of compressive residual stresses on WDE performance.

3.2.2. WDE performance of UNSM and As-M airfoil sample conditions

Similar to the WDE investigations on the flat T-shaped samples, As-M and UNSM-treated airfoil samples were studied. However, the WDE tests were conducted perpendicular to the UNSM-treated surface and a shower head nozzle of 460 μm droplet size was used. Fig. 15a and b show a schematic illustration of the WDE testing direction with respect to the airfoil treated surface and a typically eroded UNSM airfoil, respectively. The nozzle contained 13 orifices where water droplets are introduced. Due to the difficulty in accurately accounting for the number of impingements when using a shower head, the number of cycles was used.

Fig. 16 shows the WDE curves for the As-M and UNSM airfoil samples and Fig. 17 shows the corresponding ER_{inst} curves tested at different impact speeds. Fig. 16a shows that at 350 m/s, both conditions had the same initial mass losses but after additional number of cycles, the UNSM showed more mass loss as compared with the As-M condition. This can be attributed to the severity of the test which induced high stresses. Due to the work hardened surface, the material is most likely to fail in a brittle manner, allowing cracks to propagate easily. Ma et al. [15] stated that strain-hardened surfaces decrease the erosion resistance due increase in brittleness. This could be the reason for the observed mass loss in the UNSM. This observed trend is also shown in Fig. 17a where the UNSM condition showed higher maximum ER_{inst} than the As-M condition. Fig. 16b shows that at 300 m/s, both conditions showed initial mass losses but the UNSM condition further lost material with additional cycles. Interestingly, the UNSM started showing better WDE performance than the As-M condition. This is demonstrated clearly in the region A of Fig. 17b where the UNSM treatment mitigated further erosion damage. Similar tests were carried out using 300 m/s and similar trends were observed. Here, the induced compressive residual stresses might have arrested crack propagations similar to the crack arrest in stress corrosion cracking (SCC) tests [20]. Another reason for this behaviour could be attributed to the effectiveness of the UNSM treatment further away from the leading edge.

3.2.3. Effect of sample geometry and UNSM on WDE performance

The effect of UNSM process on WDE performance of treated and untreated T-shaped and airfoil samples is reported in this work. UNSM process induced compressive residual stresses, modified the microstructure as well as improved the microhardness. For the T-shaped flat sample, the WDE test was conducted parallel to the ultrasonically modified surface. UNSM condition showed enhanced WDE performance especially at speeds of 250, 275 and 300 m/s compared with the As-M condition for this sample geometry. This is clearly demonstrated in Figs. 12, 13 and 14. This behaviour is attributed to the modified microstructure and enhanced microhardness. However, at 350 m/s both treated and untreated conditions had similar WDE performances. Even though UNSM induced compressive residual stresses which are beneficial in retarding crack initiation and propagation, this benefit could not be guaranteed for the T-shaped flat samples. This is because the modified microstructure and enhanced microhardness have more profound influence on erosion resistance than induced compressive residual stresses. Hence, it can be inferred that for the flat samples, the improved WDE performance is attributed to the hardening effect only. For the airfoils where the WDE test perpendicular to the treated surface (Fig. 15a and b), the induced compressive residual stresses showed limited beneficial effect in mitigating erosion at the advanced erosion stage. This is the case at relatively low speed of 300 m/s. However, at 350 m/s where the test condition is severe, the induced compressive residual stresses showed no beneficial effect on the airfoil geometry. Contrary to the flat samples, the WDE performance of the treated airfoil condition at relatively low speed (300 m/s) could have been influenced by the induced compressive residual stresses. This is due to the fact that compressive residual stresses are through the thickness of the airfoil. It is worth noting that at 350 m/s, UNSM and its attributes were not realized on both sample geometries. This is due to the diminished effect of the UNSM treatment at high impact speed.

3.3. Optical macrographs

Optical macrographs were acquired after each interval during testing. Fig. 18 shows the erosion process of As-M and UNSM conditions at 250, 275, 300 and 350 m/s corresponding to the WDE results presented in Fig. 12. Normally, the erosion initiation process emerges with an erosion trace line due to impingement of droplets [15,48]. For instance, Fig. 18a shows a trace line on the UNSM-treated condition after 20 mins of exposure at 250 m/s. This indicates that the erosion is still in the incubation period where the mass loss is negligible [10]. Compared with the As-M condition after the same 20 min exposure in Fig. 18a, the As-M condition showed formation of small isolated pits along the trace line, thus indicating early stage of the erosion damage even though the

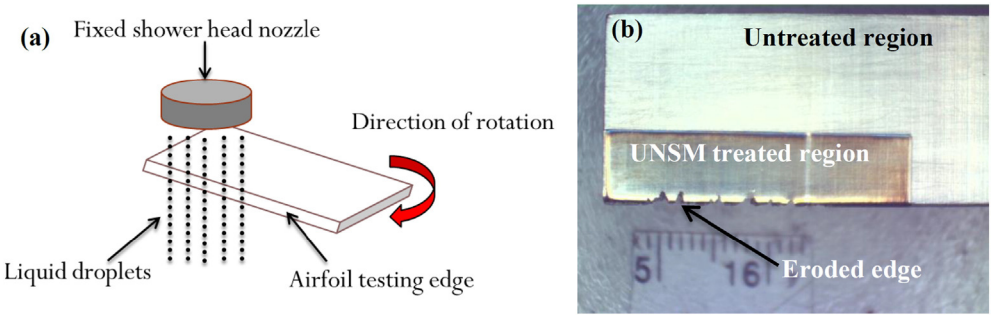

Fig. 15. (a) Schematic illustration of the WDE testing direction with respect to the airfoil treated surface and (b) typical eroded UNSM airfoil.

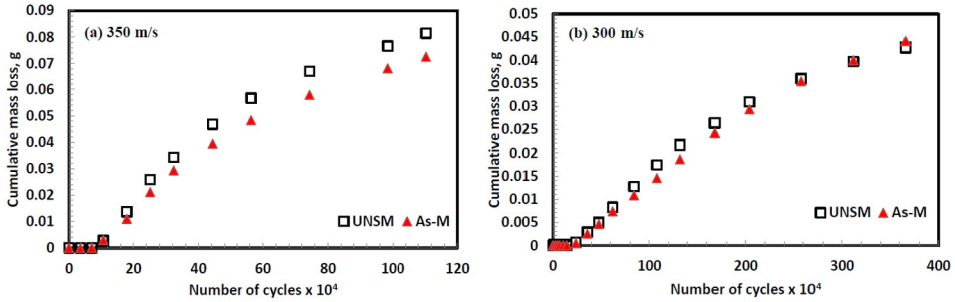

Fig. 16. WDE curves of As-M and UNSM airfoil samples at different impact speeds.

mass loss was negligible. With additional impacts, large isolated pits were formed and gradual pit growth was observed on the As-M condition. This is the situation seen in Fig. 18a after 38 mins of exposure where mass loss of 0.0003 g was recorded. At this point, the UNSM-treated condition only showed the erosion trace line without any noticeable pits. After 80 mins of exposure, the As-M condition showed a mass loss of 0.0043 g with a complete crater formed. At the same time, the UNSM condition showed only a gradual growth of isolated pits with a mass loss of 0.0001 g. The delay in erosion process on the UNSM further delayed reaching the maximum ER_{inst} and final steady state. For instance, from Fig. 14d, the As-M condition showed maximum ER_{inst} of 0.00014 g/min after 80 mins and the UNSM showed maximum ER_{inst} of 0.00013 g/min after 160 mins. Fig. 18a also confirms the enhanced WDE performance (delayed erosion initiation) of UNSM as compared with the As-M condition. Reaching the maximum erosion rate, material damage was at its peak and complete crater has been formed. The material damage was due to the high exerted pressure and the liquid lateral jetting. This jetting also interacts with surface imperfections [51], forming surface cracks and surface asperities. This leads to significant material removal during the advanced erosion stages. It is important to note that with increased exposure time, both the depth and the width of the craters are increased [15]. For instance, crater width of <1 mm and >1 mm were observed on the UNSM condition after 80 and 340 mins, respectively, as can be seen in Fig. 18a. This observation is also true when comparing the crater width/depth for different speeds at the same exposure. Similar erosion evolution and progression was observed at 275 m/s (Fig. 18b) where UNSM showed delayed erosion initiation and smaller maximum ER_{inst} than that of the As-M condition. Similar analyses were made on Fig. 18c (300 m/s) and d (350 m/s). Based on Fig. 18a–d, it can be said that at impact speeds of 250 and 275 m/s, the UNSM condition showed delayed erosion initiation and the subsequent stages as compared with the As-M condition. At impact speeds of 300 and 350 m/s, the erosion initiation and progression of the As-M and the UNSM conditions are much faster as compared with these at speeds of 250 and 275 m/s.

In a similar fashion, the As-M and UNSM airfoil samples were observed under the optical microscope during test interruptions. However, for this sample geometry, the images were taken at two different orientations considering the fact that the WDE tests were conducted perpendicular to the UNSM treated surfaces. Fig. 19 shows the erosion evolution and progression of the airfoil samples at 300 m/s. Both conditions showed similar erosion initiation as discussed previously and demonstrated in Figs. 16b and 17b. It can be seen that after 90 mins of exposure, individual craters are merging into one another due to the continuous impacts and liquid jetting. Also, the formed craters are becoming deeper as seen after 90 mins. With further exposure, the craters further deepen and widen due to the accumulated liquid impacts and the radial outflows. The increase in depth with increase in exposure can be seen more clearly in this geometry than in the T-shaped flat samples. Similar to the flat samples, increasing the impact speed showed faster erosion initiation and greater maximum ER_{inst} (Figs. 16a and 17a).

4. Conclusions

This work investigates the effect of UNSM treatment on the WDE performance of Ti—6Al—4V for the first time. The following conclusions can be drawn:

- UNSM treatment reveals surface features such as microdimples and microtracks due to the ball impact during processing. Also, the treatment induces compressive residual stress. In this work, compressive residual stresses were induced into the material down to 0.25 mm after UNSM processing.
- UNSM is associated with excessive plastic deformation, thus the process reveals mechanical deformation marks. This resulted in significant changes on the surface and sub-surface layers which leads to variation in grain size across the depth of the modified layer. Hence, material properties such as microhardness are enhanced.
- WDE results show that increasing the impact speed leads to faster erosion initiation and greater ER_{max}. This trend is attributed to the increasing impact pressure and the lateral jetting of the liquid droplet.
- UNSM T-shaped flat condition shows enhanced WDE performances especially at speeds of 250, 275 and 300 m/s compared with the As-M condition. This is attributed to the refined microstructure and increased microhardness. At speed of 350 m/s, the UNSM and As-M conditions show similar WDE performance.
- UNSM and As-M airfoils show similar WDE performance at 350 m/s, suggesting that the effectiveness of the UNSM treatment diminishes

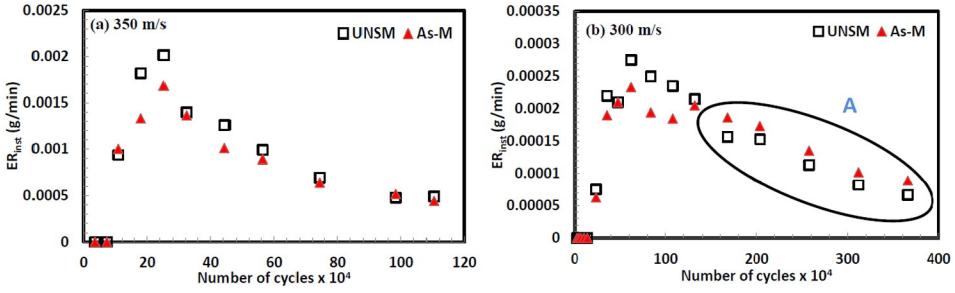

Fig. 17. ER_{inst} for As-M and UNSM airfoil samples at different impact speeds.

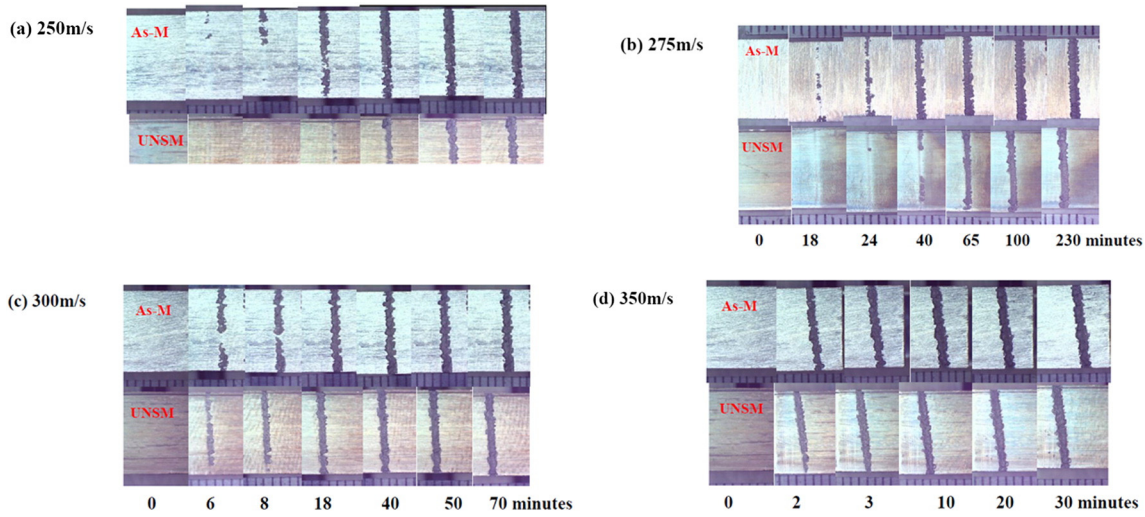

Fig. 18. Optical macrographs showing the erosion evolution and progression of As-M and UNSM flat samples tested at various speeds and exposure times.

due to test severity. However, at 300 m/s, UNSM airfoil mildly enhances WDE performance at the advanced stage of erosion damage compared with the As-M condition.

- This work concludes that for the mechanical treatment to be effective in enhancing WDE performance, surface hardening and grain refinement must be realized. Compressive residual stresses alone are not

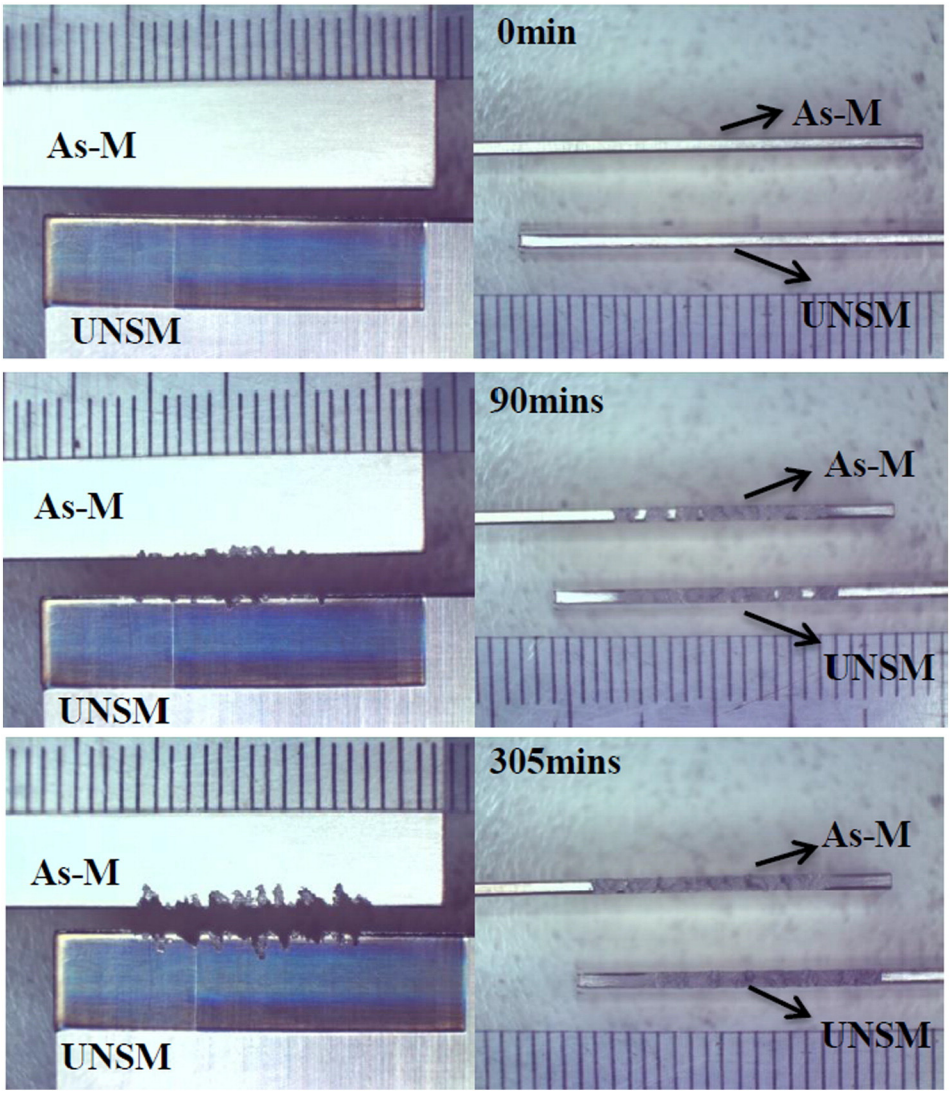

Fig. 19. Optical macrographs showing the erosion evolution and progression of As-M and UNSM airfoil samples at 300 m/s.

sufficient to enhance WDE performance especially for the T-shaped flat geometry.

Acknowledgement

Authors Abdullahi K. Gujba and M. Medraj gratefully acknowledge the financial support provided by Concordia University, Montreal, Canada (Frederick Lowy Scholars Fellowship Award, Graduate Student Support Program (GSSP) - Grant Number VE0103 and Research Assistantship (RA) - Grant Number L00264 Funds). Authors Zhencheng Ren, Yalin Dong and Chang Ye also acknowledge the start-up grants (Grant number 207135, 207137) from the College of Engineering at The University of Akron, Ohio, USA.

References

[1] J.R. Khan, Fog Cooling, Wet Compression and Droplet Dynamics in Gas Turbine Compressors, University of New Orleans, USA, 2009 PhD dissertation.
[2] ASTM G40-15, Standard Terminology Relating to Wear and Erosion, ASTM International, West Conshohocken, PA, 2015 Available online: www.astm.org.
[3] F.G. Hammitt, F.J. Heymann, Liquid-erosion failures, failure analysis and prevention, ASM Handbook, ASM International, vol. 11, 1986, pp. 163–171.
[4] F.J. Heymann, Erosion by liquids, Mach. Des. (1970) 118–124.
[5] F.J. Heymann, Liquid impingement erosion, ASM Handbook, vol. 18, ASM International, Materials Park. OH 1992, pp. 221–232.
[6] A. Thiruvengadam, S.L. Rudy, Experimental and analytical investigations on multiple liquid impact erosion, National Aeronautics and Space Administration Contractor Report (NASA CR - 1288) 1969, pp. 1–93.
[7] F.J. Heymann, On the Time Dependence of the Rate of Erosion due to Impingement or Cavitation. ASTM STP 408, American Society for Testing and Materials, 1967 70–110.
[8] V.A. Ryzhenkov, A.I. Lebedeva, A.F. Mednikov, Erosion wear of the blades of wet-steam turbine stages: present state of the problem and methods for solving it, Therm. Eng. 58 (9) (2011) 713–718.
[9] C.T. Kwok (Ed.), Laser Surface Modification of Alloys for Corrosion and Erosion Resistance, 1st editionWoodhead Publishing 2012, pp. 155–174.
[10] ASTM G73-10, Standard Test Method for Liquid Impingement Erosion Using Rotating Apparatus, ASTM International, West Conshohocken, PA, 2010 Available online: www.astm.org.
[11] M.S. Mahdipoor, F. Tarasi, C. Moreau, A. Dolatabadi, M. Medraj, HVOF sprayed coatings of nano-agglomerated tungsten-carbide/cobalt powders for water droplet erosion application, Wear 330–331 (2015) 338–347.
[12] B.S. Mann, V. Arya, An experimental study to correlate water jet impingement erosion resistance and properties of metallic materials and coatings, Wear 253 (5–6) (2002) 650–661.
[13] B.S. Mann, Water droplet and cavitation erosion behavior of laser treated stainless steel and titanium alloy: their similarities, J. Mater. Eng. Perform. 22 (12) (2013) 3647–3656.
[14] C. Gerdes, A. Karimi, H. Bieler, Water droplet erosion and microstructure of laser nitrided Ti-6Al-4V, Wear 186–187 (1995) 368–374.
[15] D. Ma, A. Mostafa, D. Kevorkov, P. Jedrzejowski, M. Pugh, M. Medraj, Water impingement erosion of deep-rolled Ti64, Metals 5 (3) (2015) 1462–1486.
[16] S. Hattori, Effects of impact velocity and droplet size on liquid impingement erosion, International Symposium on the Ageing Management & Maintenance of Nuclear Power Plants (ISaG 2010), Tokyo, Japan, 27–28th May 2010, pp. 58–71.
[17] N. Kamkar, Water Droplet Erosion Mechanisms of Ti-6Al-4V, École de Technologie Supérieure (ÉTS), Montreal, QC, Canada, 2014 PhD Dissertation.
[18] S. Hattori, M. Takinami, Comparison of cavitation erosion rate with liquid impingement erosion rate, Wear 269 (3–4) (2010) 310–316.
[19] A.K. Gujba, L. Hackel, D. Kevorkov, M. Medraj, Water droplet erosion behaviour of Ti-6Al-4V and mechanisms of material removal at the early and advanced stages, Wear 358–359 (2016) 109–122.
[20] A.K. Gujba, M. Medraj, Laser peening process and its impact on materials properties in comparison with shot peening and ultrasonic impact peening, Materials 7 (12) (2014) 7925–7974.
[21] A. Amanov, I.S. Cho, D.E. Kim, Y.S. Pyun, Fretting wear and friction reduction of CP titanium and Ti–6Al–4V alloy by ultrasonic nanocrystalline surface modification, Surf. Coat. Technol. 207 (2012) 135–142.
[22] I.S. Cho, J. Park, Y. Jeon, Fatigue behaviour of Ti-6Al-4V alloy under combined low and high cycle and ultrasonic loading, Int. J. Mater. Prod. Technol. 48 (2014) 18–33.
[23] X. Ye, Y. Ye, G. Tang, Effect of electropulsing treatment and ultrasonic striking treatment on the mechanical properties and microstructure of biomedical Ti-6Al-4V alloy, J. Mech. Behav. Biomed. Mater. 40 (2014) 287–296.
[24] A. Amanov, J. Kim, Y. Pyun, T. Hirayama, M. Hino, Wear mechanisms of silicon carbide subjected to ultrasonic nanocrystalline surface modification technique, Wear (2014) 1–9.
[25] A. Cherif, Y. Pyoun, B. Scholtes, Effects of ultrasonic nanocrystal surface modification (UNSM) on residual stress state and fatigue strength of AISI 304, J. Mater. Eng. Perform. 19 (2) (2010) 282–286.
[26] B. Wu, P. Wang, Y.S. Pyoun, J. Zhang, R. Murakami, Study on the fatigue properties of plasma nitriding S45C with a pre-ultrasonic nanocrystal surface modification process, Surf. Coat. Technol. 216 (2013) 191–198.
[27] K.Y. Zhang, Y.S. Pyoun, X.J. Cao, B. Wu, R. Murakami, Fatigue properties of SUS 304 stainless steel after ultrasonic nanocrystal surface modification (UNSM), International Journal of Modern Physics: Conference Series, vol. 6, 2012, pp. 330–335.
[28] M. Yasuoka, P. Wang, K. Zhang, Z. Qiu, K. Kusaka, Y.S. Pyoun, R. Murakami, Improvement of the fatigue strength of SUS304 austenite stainless steel using ultrasonic nanocrystal surface modification, Surf. Coat. Technol. 218 (2013) 93–98.
[29] S.J. Hong, G.H. Hwang, W.K. Han, S.G. Kang, Cyclic oxidation behavior of Pt-modified aluminide coating treated with ultrasonic nanocrystal surface modification (UNSM) on Ni-based superalloy, Surf. Coat. Technol. 205 (8–9) (2011) 2714–2723.
[30] A. Amanov, O.V. Penkov, Y.S. Pyun, D.E. Kim, Effects of ultrasonic nanocrystalline surface modification on the tribological properties of AZ91D magnesium alloy, Tribol. Int. 54 (2012) 106–113.
[31] C. Ye, A. Telang, A.S. Gill, S. Suslov, Y. Idell, K. Zweiacker, J.M.K. Wiezorek, Z. Zhou, D. Qian, S.R. Mannava, V.K. Vasudevan, Gradient nanostructure and residual stresses induced by ultrasonic nano-crystal surface modification in 304 austenitic stainless steel for high strength and high ductility, Mater. Sci. Eng. A 613 (2014) 274–288.
[32] A. Amanov, Y.S. Pyun, S. Sasaki, Effects of ultrasonic nanocrystalline surface modification (UNSM) technique on the tribological behavior of sintered Cu-based alloy, Tribol. Int. 72 (2014) 187–197.
[33] ASM aerospace specification metals: Titanium Ti-6Al-4V (Grade 5). ASM Material Data Sheet. Available online: www.aerospacemetals.com (as viewed in July 2015).
[34] S. Spanrad, J. Tong, Characterisation of foreign object damage (FOD) and early fatigue crack growth in laser shock peened Ti–6Al–4V aerofoil specimens, Mater. Sci. Eng. A 528 (4–5) (2011) 2128–2136.
[35] M.E. Hilley (Ed.), Residual Stress Measurement by X-ray Diffraction - (SAE) J784a: Report of Iron and Steel Technical Committee Approved September 1960 and Last Revised by Fatigue Design and Evaluation Committee August 1971, Society of Automotive Engineers 1971, pp. 1–119.
[36] L.M. Gammon, R.D. Briggs, J.M. Packard, K.W. Batson, R. Boyer, C.W. Domby, Metallography and microstructures of titanium and its alloys, ASM Handbook, vol. 9, 2004, pp. 899–917.
[37] M.S. Mahdipoor, H.S. Kirols, D. Kevorkov, P. Jedrzejowski, M. Medraj, Influence of impact speed on water droplet erosion of TiAl compared with Ti6Al4V, Sci. Rep. 5 (2015), 14182 17 pp.
[38] M. Ahmad, M. Casey, N. Sürken, Experimental assessment of droplet impact erosion resistance of steam turbine blade materials, Wear 267 (9–10) (2009) 1605–1618.
[39] A. Amanov, S. Sasaki, Frictional behavior of duplex nano-corrugated and nanostructured Cu alloy produced by UNSM, Procedia Eng. 68 (2013) 491–496.
[40] A. Amanov, I.S. Cho, D.E. Kim, Effectiveness of high-frequency ultrasonic peening treatment on the tribological characteristics of Cu-based sintered materials on steel substrate, Mater. Des. 45 (2013) 118–124.
[41] N. Al-Aqeeli, K. Abdullahi, A.S. Hakeem, C. Suryanarayana, T. Laoui, S. Nouari, Synthesis, characterisation and mechanical properties of SiC reinforced Al based nanocomposites processed by MA and SPS, Powder Metall. 56 (2) (2013) 149–157.
[42] N. Al-Aqeeli, K. Abdullahi, C. Suryanarayana, T. Laoui, S. Nouari, Structure of mechanically milled CNT-reinforced Al-alloy nanocomposites, Mater. Manuf. Process. 28 (9) (2013) 984–990.
[43] K. Abdullahi, N. Al-Aqeeli, Mechanical alloying and spark plasma sintering of nano-Sic reinforced Al–12Si–0.3Mg alloy, Arab. J. Sci. Eng. 39 (4) (2014) 3161–3168.
[44] I.A. Chou, H.M. Chan, M.P. Harmer, Machining induced surface residual stress behavior in Al_2O_3-SiC nanocomposites, J. Am. Ceram. Soc. 79 (1996) 2403–2409.
[45] A. Amanov, I.S. Cho, Y.S. Pyoun, C.S. Lee, I.G. Park, Micro-dimpled surface by ultrasonic nanocrystal surface modification and its tribological effects, Wear 286–287 (2012) 136–144.
[46] A. Amanov, Y.S. Pyoun, I.S. Cho, C.S. Lee, I.G. Park, The evaluation of the micro-tracks and micro-dimples on the tribological characteristics of thrust ball bearings, J. Nanosci. Nanotechnol. 11 (2011) 701–705.
[47] Y. Zaden, V. Songmene, R. Khettabi, J. Masounave, Surface integrity of Al6061-T6 drilled in wet, semi-wet and dry conditions, Proceedings of the 37th International MATADOR Conference, Manchester, UK, July 25–27th 2012, pp. 131–134.
[48] H.S. Kirols, D. Kevorkov, A. Uihlein, M. Medraj, The effect of initial surface roughness on water droplet erosion behaviour, Wear 342–343 (2015) 198–209.
[49] G. Hoff, G. Landbein, H. Rieger, Material destruction due to liquid impact in erosion by cavitation or impingement, A Symposium Presented at the 6–9th Annual Meeting, American Society for Testing and Materials, Atlanta City, New Jersey, 26th Jun.–1st Jul. 1966, pp. 42–69.
[50] T. Sanada, K. Ando, T. Colonius, A computational study of high-speed droplet impact, Fluid Dyn. Mater. Process. 7 (4) (2011) 329–340.
[51] S. Honghui, J.E. Field, Stress waves propagation in solids under high-speed liquid impact, Sci. China, Ser. G 47 (6) (2004) 752–766.
[52] J.E. Field, The physics of liquid impact, shock wave interactions with cavities, and the implications to shock wave lithotripsy, Phys. Med. Biol. 36 (11) (1991) 1475–1484.
[53] F.J. Heymann, High speed liquid impact between a liquid drop and a solid surface, J. Appl. Phys. 40 (13) (1969) 5113–5122.
[54] S. Yerramareddy, Effect of operational variables, microstructure and mechanical properties on the erosion of Ti-6Al-4V, Wear 142 (1) (1991) 253–263.
[55] N. Yasugahira, K. Namura, R. Kaneko, T. Satoh, Erosion resistance of titanium alloys for steam turbines blades as measured by water droplet impingement, Titanium Steam Turbine Blading, PaloAlto, 2988, Pergamo, New York 1990, pp. 385–401.
[56] J.I. Robinson, R.C. Reed, Water droplet erosion of laser surface treated Ti-6Al-4V, Wear 187 (1995) 360–367.